Available online at www.sciencedirect.com

ScienceDirect

Biochimica et Biophysica Acta 1778 (2008) 1344–1355

Biochimica et Biophysica Acta BBA

www.elsevier.com/locate/bbamem

Molecular organization of the lipid matrix in intact *Stratum corneum* using ATR-FTIR spectroscopy

Mila Boncheva *, Fabienne Damien, Valéry Normand

Corporate R&D Division, Firmenich SA, P.O. Box 239, Route des Jeunes 1, CH-1211 Geneva 8, Switzerland

Received 27 November 2007; received in revised form 22 January 2008; accepted 28 January 2008
Available online 11 February 2008

Abstract

ATR-FTIR spectroscopy is useful in investigating the lateral organization of *Stratum corneum* (SC) lipids in full-thickness skin. Based on studies of the thermotropic phase transitions in *n*-tricosane and in excised human skin, the temperature dependence of the CH_2 scissoring bandwidth emerged as a measure of the extent of orthorhombic and hexagonal phases. This dependence provides a simpler measure of the lateral order in lipid assemblies than the common spectroscopic approaches based on difference spectra, curve fitting of the CH_2 scissoring region, and the position of the CH_2 stretching vibrations. It has the advantages of ease of determination, relatively low variability, and high discriminative power for the type of lateral intermolecular chain packing. A comparison of the lateral organization of the lipids at the SC surface of mammalian skin using the scissoring bandwidth revealed considerable differences between human abdominal skin (containing mostly orthorhombic phases), porcine ear skin (containing mostly hexagonal phases), and reconstructed human epidermis (containing mostly disordered phases). This parameter also correctly described the different effects of propylene glycol (minimally disturbing) and oleic acid (formation of a highly disordered phase) on the SC lipids in excised human skin. The procedure described here is applicable to *in vivo* studies in the areas of dermatology, transdermal drug delivery, and skin biophysics.

Keywords: Human skin; Infrared spectroscopy; Lipid organization; Skin biophysics

1. Introduction

The objective of this work was to develop a method to evaluate the molecular organization of the lipid matrix in intact (*i.e.*, not separated from the underlying skin strata) *Stratum corneum* (SC). The procedure we propose is based on second-derivative ATR-FTIR spectroscopy and uses the CH_2 scissoring bandwidth as a measure of the lateral chain packing. We demonstrate the application of this parameter to compare the molecular organization of SC lipids in human, porcine, and reconstructed skin, and to estimate the changes of the molecular organization following topical application of chemicals.

SC, the topmost layer of the skin, consists of anucleated cells (corneocytes) filled with keratin filaments and embedded in a lipid matrix that is heterogeneous in composition and structure [1,2]. The molecular organization of the SC lipids is important in maintaining the barrier properties of the skin [3]. It has been extensively studied by X-ray diffraction [1,4], IR spectroscopy [5–7], DSC [8], ^2H NMR spectroscopy [9], and electron microscopy [10]. Most of the experimental evidence is consistent with the domain mosaic model proposed by Forslind, in which the lipids are organized in ordered domains connected by lipids in a disordered phase [11,12]. The existence of lipids in ordered (orthorhombic, OR, and hexagonal, HEX) and disordered (liquid-crystalline, LIQ) phases has been demonstrated in isolated SC (for a review, see [8]), and in model mixtures of SC lipids (*i.e.*, ceramides, free fatty acids, and cholesterol) [13–16]. While the exact localization of the three phases in mammalian SC is still debatable, numerous studies have shown that the permeability for water [17,18] and small molecules [5,19,20] in healthy skin differs considerably from that in diseased or perturbed skin with altered composition and phase content (for a review, see [1] and the references therein).

Fig. 1 shows schematically the chain conformation and the lateral chain packing in the three phases, together with their

* Corresponding author. Tel.: +41 22 780 3027; fax: +41 22 780 3334.
E-mail address: mila.boncheva@firmenich.com (M. Boncheva).

0005-2736/$ - see front matter © 2008 Elsevier B.V. All rights reserved.
doi:10.1016/j.bbamem.2008.01.022

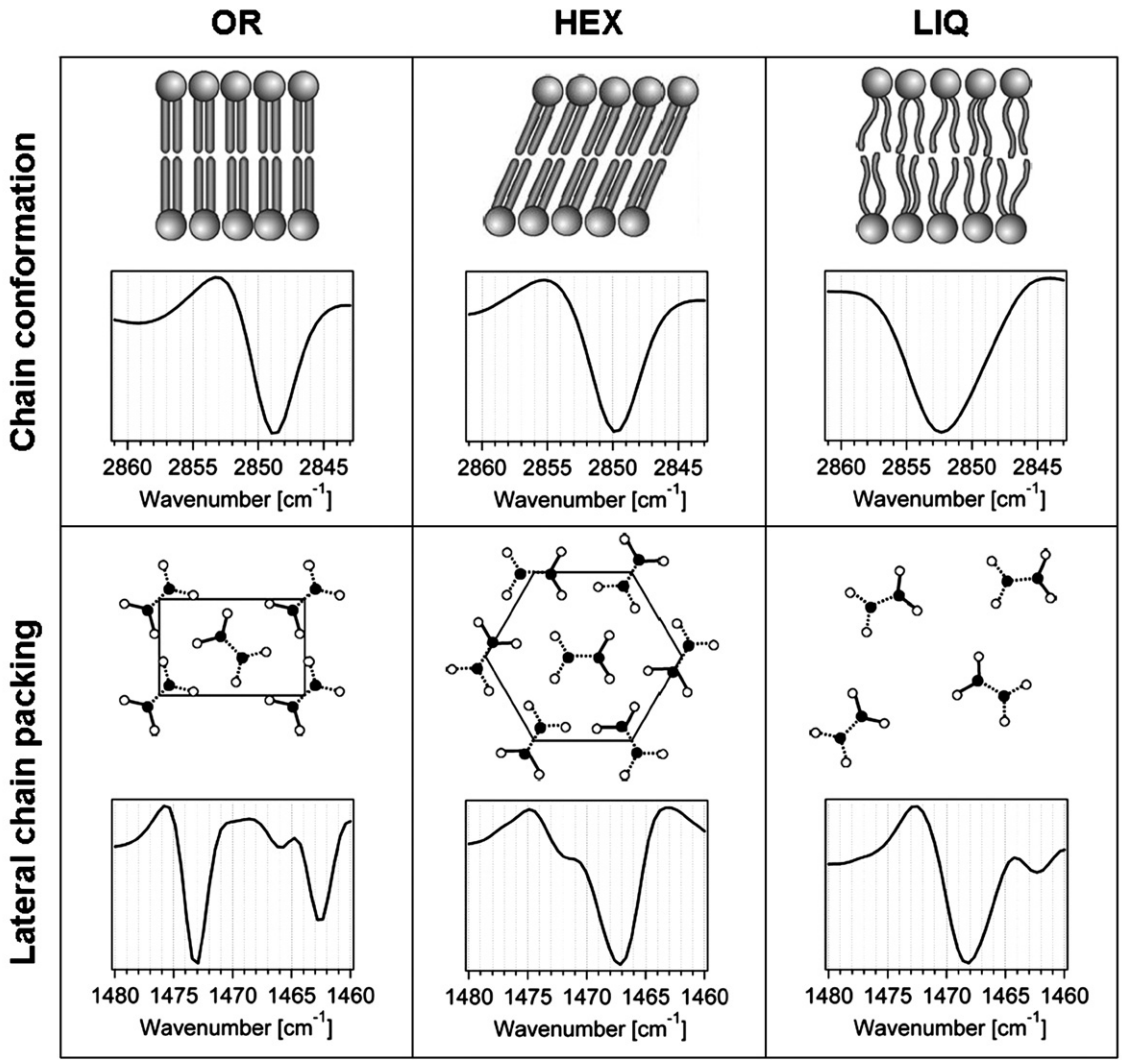

Fig. 1. Molecular organization of SC lipids. Scheme of the chain conformation (top row) and lateral chain packing (bottom row) in orthorhombic (OR), hexagonal (HEX), and liquid-crystalline (LIQ) phases of long-chain lipids, together with the characteristic IR features in the CH_2 symmetric stretching (top row) and the CH_2 scissoring (bottom row) regions of their second-derivative spectra.

characteristic IR features. In the OR phase, the aliphatic chains adopt all-*trans* conformation and are organized in a rectangular crystalline lattice. In the HEX phase, the all-*trans* aliphatic chains are tilted in respect to the crystal plane, and are organized in a less dense, hexagonal lattice. In the LIQ phase, the chains exhibit a high degree of *gauche* isomerization, and the lateral organization is entirely lost. The chain conformation and the lateral packing in the three phases are easily discernible by IR spectroscopy. The position and the bandwidth of the CH_2 symmetric stretching band are sensitive markers of the chain conformational order: the increased rotational motion of the alkyl chains during the OR–HEX transition and the introduction of *gauche* defects in the chains during the HEX–LIQ transition lead to broadening of the band and its shift to higher wavenumbers. Splitting of the CH_2 rocking (~720 cm^{-1}) and the scissoring modes (~1468 cm^{-1}) into two, separate bands is a characteristic IR signature for the presence of OR phases. The magnitude of the band separation is indicative of the degree of inter-chain interactions and of the size of the domains with OR organization: the two bands get closer during melting, and in purely HEX phases they coalesce into a single band [21–23]. The rocking mode occurs in a region free from other IR-active modes originating from the lipid chains [24,25]. In full-thickness skin, however, this spectral region is dominated by the extremely strong absorbance of the water libration band [7]. In contrast, the scissoring mode occurs very close to the CH_3 bending mode, which in SC originates mostly from the skin keratins and is fairly strong. Its factor group splitting in OR phases can, however, be observed in difference and second-derivative spectra even in well-hydrated samples [25–27].

Recently, two elegant works from the labs of R. Mendelsohn and D. Moore used transmission FTIR spectroscopy to follow the kinetics of formation of OR domains in model mixtures of SC lipids [28] and in isolated SC [29]. These studies suggested the kinetics of recovery of the CH_2 rocking and scissoring modes as a direct spectroscopic probe for the *rate of skin barrier reformation* following thermal perturbation. Here, we address a complementary question relating to the skin barrier organization

and function: we aim to establish a spectroscopic probe for the *extent of lateral organization* of the lipids in intact SC and the *degree of its perturbation*.

Our method of choice was ATR-FTIR spectroscopy, as this technique can provide structural information localized in a surface layer of limited thickness and is, thus, applicable to *in vivo* and *ex vivo* studies of full-thickness skin. Previously, it has been used to study the lipid conformational order, the hydration state, and the penetration of substances in intact human and animal SC [30–38]. Here, we extend its use to evaluate the amount of OR and HEX phases present in the samples by measuring the magnitude of the band splitting in the CH_2 scissoring mode. Instead of the procedures commonly used to evaluate the CH_2 scissoring split–based on difference spectra [23,26,27], spectrum deconvolution [25], and curve fitting [26,39]–we used the width of the second-derivative spectra in the region ~1475–1460 cm^{-1}. In simple systems of *n*-alkanes, the absorbance of the CH_2 scissoring mode is much stronger than the one of the neighboring CH_3 bending mode; the magnitude of the scissoring split can, therefore, be unambiguously calculated by establishing the exact positions of the two peaks in difference spectra. In a complex system like the skin–one comprising numerous classes of lipids and displaying a strong CH_3 bending mode in the immediate vicinity of the CH_2 scissoring mode–it is difficult to estimate the exact positions of the two scissoring components from difference spectra; spectral deconvolution and curve fitting are often not straightforward, and are time-consuming procedures [40]. Here, we first validated the use of the bandwidth for detection of the phase transitions in *n*-tricosane, a system with well characterized thermotropic phase behavior [39,41]. Furthermore, we demonstrated that the thermal behavior of the scissoring bandwidth adequately describes the solid–solid phase transition of lipids in excised human skin as compared to the procedures based on difference spectra, curve fitting, and the positions of the CH_2 stretching bands. We next demonstrated the use of this criterion to compare the thermotropic behavior and extent of OR phase in the topmost surface layer of intact SC from excised human and porcine skin, and from reconstructed skin. Finally, we showed its applicability to evaluate the effect of two widely used penetration enhancers–propylene glycol, PG [42] and oleic acid, OA [43]–on excised human skin.

The procedure we describe offers a convenient, easily accessible semi-quantitative probe of the lateral organization of lipids in intact SC. It is well suited to address questions pertinent to the areas of transdermal drug delivery, dermatology, and skin biophysics, such as the inter- and intra-species variations and depth profile of the lipid organization in SC, and the changes in the molecular organization induced by environmental conditions (*e.g.*, temperature and humidity) or by topical application of products.

2. Materials and methods

2.1. Skin samples

We obtained dermatomed human abdominal skin (Caucasian donors aged between 41 and 63) collected during cosmetic surgery (nominal thickness 300–500 μm) from Biopredic International (Nice, France) and from Epithelix Sàrl (Plan les Ouates, Switzerland). The skin was stored frozen at −20 °C (wrapped in Parafilm and packed in ZipLock bags) for not longer than 4 months prior to use.

We collected the ears of domestic pigs at the local slaughterhouse (Gland, Switzerland) 2–3 h after the animals were sacrificed. After thoroughly washing the ears with cold water, we removed the skin from the outer sides of the ears using a scalpel, clipped the hairs using hair clippers, and dermatomed the skin to a thickness of 350–400 μm using a 50-mm electric dermatome (Nouvag AG, Goldach, Switzerland). The skin was stored frozen at −20 °C (wrapped in Parafilm and packed in ZipLock bags) for not longer than 1 month prior to use.

Before collection of ATR-FTIR spectra from both human and porcine skin, we defrosted the samples for 30 min at room temperature and wiped the SC surface 2–3 times with cotton swabs wetted with cold (4 °C) hexane, to remove traces of sebum.

We obtained samples of reconstructed skin from Epithelix Sàrl (Plan les Ouates, Switzerland). The cultures of human keratinocyte cells–isolated from abdominal biopsy of a 42-year-old patient–were grown submerged in the proprietary culture medium of the provider with one passage. Next, the epidermal equivalents were cultured for 13–15 days at the air/medium interface, and were taken out of the incubator (5% CO_2 atmosphere, 84% relative humidity, temperature 37 °C) 1 h before use. Before collecting the ATR-FTIR spectra, we carefully peeled the epidermal sheets off their filter supports, rinsed them with deionized water, and dried the excess water with KimTech tissues (Kimberly Clark Inc., USA).

2.2. Treatment of excised human skin with OA and PG

Before the treatment, we defrosted the dermatomed skin samples and cleaned their SC surface with cold hexane as described above. From each skin sample we prepared two pieces with dimensions of approximately 4×4 mm. We placed the two pieces of skin on KimTech tissues soaked with PBS buffer (150 mM, pH 7.4). On top of one of the pieces we placed a cotton swab soaked in 30%-solution (w/v) of oleic acid (Alpha Aesar, Germany, purity 99%) in ethanol (Carlo Erba, Italy, purity ≥ 99.8%) or soaked in propylene glycol (Carlo Erba, Italy, *p.a.* grade), and fixed it in tight contact with the skin surface; the other piece (control sample) was kept untreated. We incubated the two pieces in an oven at 32 °C and 95% relative humidity for 4 h. At the end of the incubation period, we wiped off the excess OA or PG solution from the SC surface of the treated sample with 2–3 cotton swabs wetted with ethanol. After evaporation of the solvent, we collected FTIR spectra of the samples using ATR crystal preheated to 32 °C.

2.3. IR spectroscopy

We collected all spectra with a spectral resolution of 2 cm^{-1} using a Vertex-70 spectrometer (Bruker Optics, Germany) equipped with a narrow band MCT detector and a Golden Gate accessory (Specac, UK). The accessory was modified (Portmann Instruments AG, Switzerland) for gradual heating of the diamond surface from 26 to 100 °C with an integrated heater and a temperature controller. The temperature variations at the crystal surface did not exceed 0.2 °C at any preset temperature. The whole instrument was constantly purged with dry N_2, and the accessory—with a stream of Ar heated to approximately 26 °C. Each spectrum was an average of 200 scans, recorded with scanner velocity of 20 kHz using a Blackman-Harris 3-term apodization function, and a level of zero-filling equal to four.

To collect an IR spectrum from the skin samples, we placed the sample (cut to dimensions 4×4 mm), SC-side down, onto the diamond ATR crystal, covered it with a PTFE sheet (thickness of 0.5 mm) cut to size, for thermal isolation, and held it in place with the flat sapphire anvil. To ensure reproducible contact between the sample and the crystal, we applied always the same pressure on top of samples of the same type (torque setting of 50 cNm for human and porcine skin, and 20 cNm for reconstructed skin; according to the manufacturer, these settings correspond to a pressure of 1.5 kBar and 0.6 kBar, respectively, applied over the diamond surface), and kept the samples in place for 10 min before collecting the spectra.

To collect spectra from *n*-tricosane, we placed a small amount of powder (Fluka, purity > 99.5%) on the ATR crystal, covered it with a PTFE sheet (dimensions 3×3×0.5 mm) for thermal isolation, and held it in place with the flat sapphire anvil (torque setting of 50 cNm, corresponding to a pressure of 1.5 kBar over the diamond surface).

In the temperature studies, we heated the skin samples at the rate of 15 °C/h, and collected spectra in 2±0.3 °C increments between 28 and 90 °C (1 °C increment for the spectra collected from *n*-tricosane in the temperature interval 28–50.4 °C). During collection of the spectra (156 s per spectrum), the temperature at the diamond surface increased by ≤0.6 °C between the beginning and the end of the measurement; the values plotted in Figs. 2, 4, 6, and 8 are the mean temperatures reached during collection of one spectrum.

2.4. Data treatment

If necessary, we corrected the spectra for the spectral contribution of water vapor. For data treatment we used the instrument software OPUS 5.5. We calculated difference spectra by subtracting each spectrum from the one collected at higher temperature. To determine the position of the minima in the difference spectra we tested three commonly used procedures based on finding the absolute minimal value in selected vicinity, second derivative, or center of gravity algorithm. With all three procedures it was very difficult (and in many cases, impossible) to establish the positions of the minima, especially in spectra recorded above 45 °C. To determine the position of the CH_2 symmetric stretching band, we applied the center of gravity algorithm of the software (95% peak height) to the spectra previously baseline-corrected between 2864 and 2834 cm^{-1}; using this procedure, the uncertainty in the peak position is ≤0.02 cm^{-1} [44]. Second derivatives were calculated without smoothing of the spectra. Before calculating the scissoring bandwidth, we baseline-corrected the second-derivative spectra between the endpoints of the scissoring region (~1480–1460 cm^{-1}), and normalized them to identical minima and maxima between the two points of the baseline. We calculated the bandwidth at 50% and at 15% of the peak height (denoted as FW-50 and FW-15, respectively).

To calculate the integrated intensity of the two peaks characteristic of OR phases, we applied a curve fitting procedure (developed in Microsoft Office Excel) to series of absorbance spectra collected from the same sample at different temperatures. Before fitting, we baseline-corrected the spectra between 1480 and 1430 cm^{-1}, the spectral region comprising both the CH_2 scissoring and the CH_3 bending modes. We analyzed this spectral region as a sum of five Gaussian curves (three for the CH_2 scissoring mode and two for the CH_3 bending mode) with consecutive optimization of the amplitudes, the positions, and the widths of the individual bands. The quadratic deviation of the fits was $\leq 4.5\times10^{-5}$. We calculated the integrated intensity A of the peaks characteristic of OR phases as

$$A = \sqrt{\frac{\pi}{4\ln 2}} I_{\max} FW50,$$

where I_{max} and $FW50$ are the peak intensity and full width at half maximum, respectively, obtained in the curve fitting procedure [45]. Full details can be found in the Supplemental material.

3. Results

3.1. Solid/solid phase transitions in n-tricosane

Fig. 2 summarizes our results for the thermotropic behavior of the CH_2 scissoring mode of *n*-tricosane (Fig. 2a), estimated from difference (Fig. 2c) and second-derivative (Fig. 2d) spectra, and the position of the CH_2 symmetric stretching mode (Fig. 2b). Within the studied temperature range 28–51 °C, this alkane is known to exist in four different phases: orthorhombic (OR), face-centered orthorhombic or pseudo-hexagonal (FCO), hexagonal (HEX), and liquid (LIQ), with corresponding phase transition temperatures of ~40 °C, 45 °C, and 48 °C, respectively [39,41,46]. These phase transitions were clearly apparent in the temperature dependence of both the magnitude of the CH_2 scissoring split (calculated from the positions of the two bands in difference spectra, Fig. 2, a and c) and the position of the CH_2 symmetric stretching vibration (Fig. 2b).

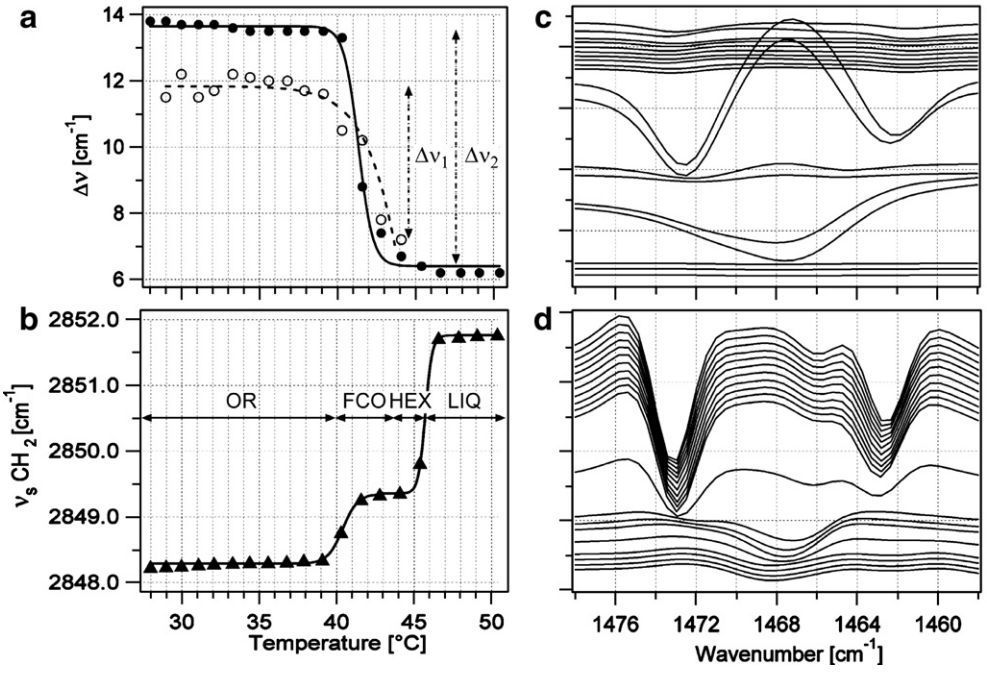

Fig. 2. Thermotropic phase transitions of *n*-tricosane. Temperature dependence of the CH_2 scissoring split and bandwidth (a) and of the position of the CH_2 symmetric stretching mode (b) in *n*-tricosane. The scissoring split with an amplitude $\Delta\nu_1$ (the open circles in a) was calculated from the positions of the two bands estimated from difference spectra (c), and the scissoring bandwidth with an amplitude $\Delta\nu_2$ (the filled circles in a)—from the full width at half maximum (FW-50) of the second-derivative spectra (d). The spectra in (c) and (d) are plotted in order of increasing temperatures from top to bottom of the panels, and are offset for clarity. The full lines in (a) and (b) represent the best fits to the experimental points: a sigmoidal curve for the scissoring bandwidth, and two sigmoidal curves for the position of the CH_2 symmetric stretching mode (comprising the temperature intervals 28–44 °C and 44–50 °C, respectively); the dashed line in (a) is for guidance of the eye only.

Within the OR phase (28–39 °C), the scissoring mode was split into two bands separated by ~12 cm^{-1} (Fig. 2c), and the CH_2 symmetric stretching mode was centered at ~2848.3 cm^{-1}. Within the FCO phase (~40–44 °C), the scissoring split was retained but its magnitude decreased continuously to a minimal value of ~6 cm^{-1}; the CH_2 symmetric stretching band shifted gradually to slightly higher wavenumbers as a result of increased rotational motions along the chains, and reached a plateau at ~2849.4 cm^{-1}. In the HEX and LIQ phases (~44–51 °C), the scissoring split disappeared completely and the two scissoring bands fused into a single one. The CH_2 symmetric stretching band underwent a further blue shift of 2.5 cm^{-1} as a result of decreased conformational order (melting) of the chains, and at the onset of the LIQ phase it reached a plateau at ~2851.8 cm^{-1}. Fig. 2a shows also the scissoring bandwidth at 50% peak height (FW-50) estimated from the second-derivative spectra plotted in Fig. 2d. The bandwidth displayed qualitatively the same temperature dependence as the magnitude of the split estimated from the difference spectra: its value was maximal and constant in the OR phase, decreased in the FCO phase, reached a minimum with the onset of the HEX phase, and retained it in the LIQ phase. Using a sigmoidal fit of the bandwidth data, we estimated the transition temperature OR-FCO to be 41.3±0.1 °C. This value is very close to the one found from fitting the CH_2 symmetric stretching data (40.4±0.1 °C), and agrees with the values reported in the literature [39,41,46].

These results demonstrate that the scissoring bandwidth estimated from second-derivative spectra is a useful spectroscopic indicator for the presence and the extent of OR phases. Importantly, the absolute change of the scissoring bandwidth ($\Delta\nu_2$ in Fig. 2a) during the transition OR–HEX was ~50% bigger than the absolute change of the scissoring split ($\Delta\nu_1$ in Fig. 2a). Thus, evaluating the extent of the OR phase is easier using the bandwidth than using the split, especially when comparing changes occurring over small temperature intervals.

3.2. Solid/solid phase transitions in SC from excised human skin

We compared the applicability of the scissoring bandwidth FW-50 to detection of the thermotropic phase transition OR–HEX of SC lipids in excised human skin with three widely used spectroscopic methods based on difference spectra and curve fitting of the CH_2 scissoring region and on the position of the symmetric CH_2 stretching mode. Fig. 3, a and b show difference and second-derivative spectra calculated from the same set of absorbance spectra collected during heating of a skin sample between 28 and 60 °C; Fig. 3c shows the absorbance spectrum of the same sample recorded at 28 °C, together with the five curves used to fit the CH_2 scissoring and CH_3 bending regions (for simplicity, we did not include here the absorbance spectra recorded at higher temperatures and the corresponding curve fits; see the Supplemental material for details).

As expected from the published data [1,8], the spectroscopic features in the CH_2 scissoring and stretching regions unquestionably indicated the presence of OR and HEX phases at 28 °C. The scissoring region contained two peaks characteristic of OR phases

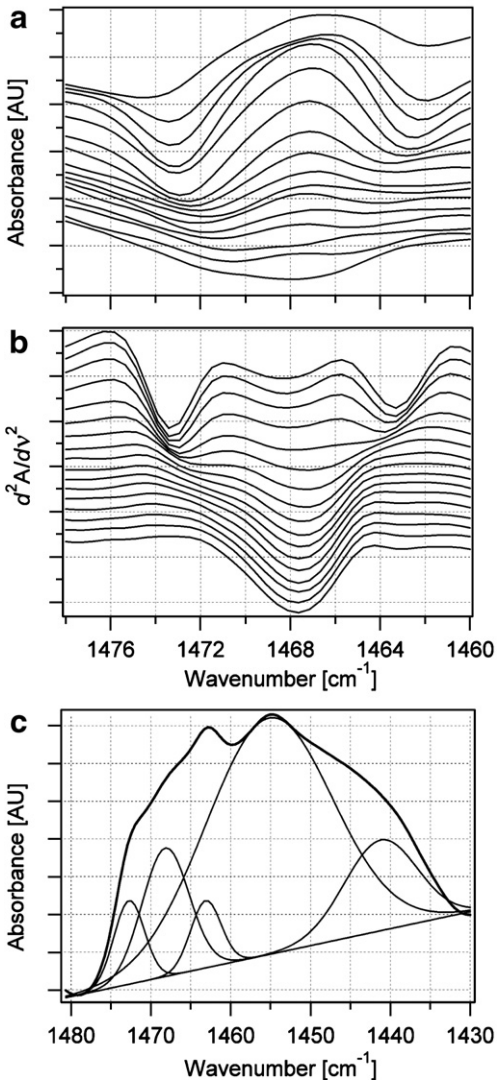

Fig. 3. Characteristic features of the CH_2 scissoring region in spectra collected from SC in excised human skin. Difference (a) and second-derivative (b) spectra calculated from absorbance spectra that were collected during heating the same skin sample from 28 to 60 °C. The spectra are plotted in order of increasing temperature from top to bottom of the panels, and are offset for clarity. (c) Absorbance spectrum of the same sample recorded at 28 °C (thick line) and the five Gaussian curves used to fit the CH_2 scissoring and the CH_3 bending regions (thin lines). See Materials and methods and the Supplemental material for details of the curve fitting procedure.

(centered at approximately 1473 and 1463 cm^{-1}) together with a peak characteristic of HEX phases (centered at approximately 1468 cm^{-1}, Fig. 3b), and the CH_2 stretching mode was centered at a typical of predominantly *trans*-arranged alkyl chains low wavenumber (2849.39 cm^{-1}; see Materials and methods for the uncertainty in determination of the peak position). Upon heating, the splitting of the CH_2 scissoring mode gradually decreased, and the CH_2 symmetric stretching mode shifted to higher wavenumbers, reflecting the complete melting of OR into HEX phases around 55–60 °C.

We attempted to determine the OR–HEX transition temperature using the temperature dependence of the scissoring split (calculated from the positions of the minima in the difference

spectra, Fig. 4a), the integrated intensity of the two peaks characteristic of OR phases (calculated using curve fitting, Fig. 4a), the position of the CH_2 symmetric stretching mode (Fig. 4b), and the scissoring bandwidth FW-50 (calculated using second-derivative spectra, Fig. 4c).

The temperature dependence of the scissoring split lacked a defined inflection point, making it difficult to estimate the specific transition temperature. Moreover, there was considerable uncertainty associated with the exact position of the peaks in the difference spectra (*i.e.*, the wavenumbers at which the maximal changes of absorbance occurred during heating): while in spectra collected at temperatures of ≤47 °C the two peaks were clearly discernible, at higher temperatures it became increasingly difficult to determine their exact positions (see Fig. 3a; we ran into the same problem with the second-derivative spectra shown in Fig. 3b).

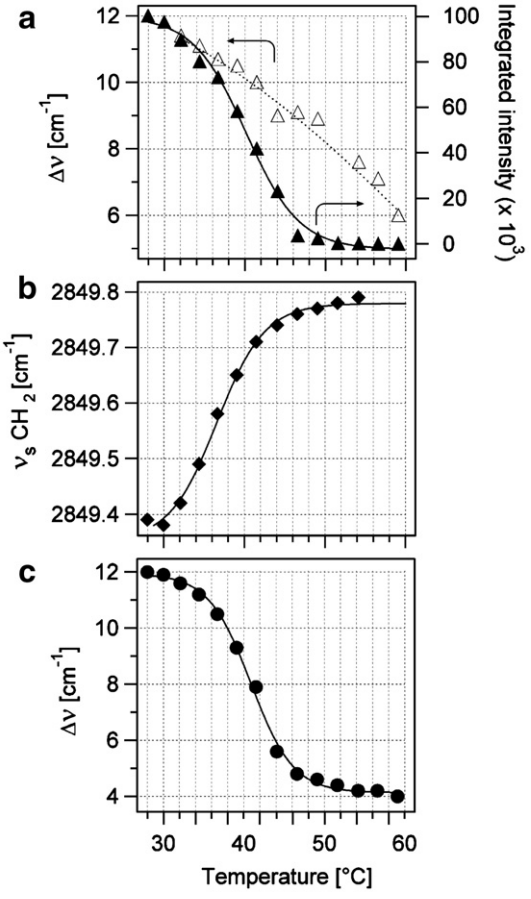

Fig. 4. Detection of the thermotropic OR–HEX phase transitions of SC lipids in excised human skin. Temperature dependence of the scissoring split (open triangles, a), the integrated intensity of the scissoring bands characteristic for OR phases calculated using curve fitting of the original absorbance spectra (closed triangles, a), the position of the CH_2 symmetric stretching band (b), and the scissoring bandwidth FW-50 (c). The dotted line connecting the data points of the scissoring split is for guidance of the eye only. The full lines in (a), (b), and (c) represent sigmoidal fits of the experimental data, with corresponding inflection points at 40±0.4 °C (integrated peak intensity), 36.6±0.3 °C (position of the CH_2 symmetric stretching band), and 40.9±0.2 °C (scissoring bandwidth FW-50). The data in the three panels were calculated from absorbance spectra collected from only one sample; see Fig. 5 for average values from multiple samples.

The temperature dependences of the integrated peak intensity, the position of the CH_2 symmetric stretching mode, and the scissoring bandwidth had sigmoidal shapes, with corresponding inflection points at 40±0.4 °C, 36.6±0.3 °C, and 40.9±0.2 °C. The difference of approximately 3 °C between the transition temperature determined using the CH_2 scissoring and stretching modes is not surprising, considering the different sensitivity of these modes to the in-plane organization of the SC lipids, and–even more importantly–the complex composition and organization of the human SC. Overall, the three methods delivered very similar values for the transition temperature, consistent with those reported in the literature for isolated human SC [26]. Using the scissoring bandwidth FW-50 to describe the OR–HEX phase transition, however, offers several advantages: (*i*) this parameter is easily accessible after only one simple transformation of the original absorbance spectra, unlike the fairly complicated fitting procedure; (*ii*) the inherent uncertainty of the FW-50 values is much smaller than the uncertainty associated with determination of the peak positions in difference and second-derivative spectra or with fitting of absorbance spectra; (*iii*) the absolute magnitude of the scissoring bandwidth (*i.e.*, the difference between its values for mostly OR and mostly HEX lateral organization), ~8 cm^{-1}, is higher than the magnitude of the scissoring split (~5 cm^{-1}) and the shift of the CH_2 symmetric stretching position (~0.4 cm^{-1}), thus facilitating the discrimination between the two phases; this last point becomes particularly important when one takes into account the typical inter-individual variations of these parameters (see Fig. 5).

In summary, this comparison demonstrates that the use of the scissoring bandwidth to describe the existence and the relative extent of OR phases can be broadened from the one-component system of long-chain alkanes (Fig. 2) to a complex system containing a mixture of different lipid classes like the SC.

An important caveat for the correct interpretation of the thermotropic changes of the scissoring bandwidth is its appropriate use for quantitative or semi-quantitative estimation of the extent of OR phase. Studies in mixtures of hydrogenated and deuterated alkanes have demonstrated a correlation between the size of the OR domains and the magnitude of the scissoring split [28,39,47]. In the simple, one-component system of *n*-tricosane, the alkyl chains are organized in a purely OR phase up to ~40 °C; thus, in this system the maximal value of the bandwidth corresponded to a 100%-content of OR phases and we could interpret its thermotropic changes quantitatively. The complexity of the human SC which contains lipids of different classes and chain lengths, however, precludes such quantitative interpretation of the scissoring bandwidth. The relative content of OR phases at physiological temperatures is still debatable. Furthermore, several investigations of isolated SC and model mixtures of SC lipids have suggested that phase-separated domains of different composition exist in human SC [26,48]; in a spectroscopic study we could not distinguish between small changes associated with all OR phases and a big change associated with only one of these phases. Thus, we could interpret the thermotropic changes of the scissoring bandwidth only in terms of relative changes of the phase content in respect to its initial state.

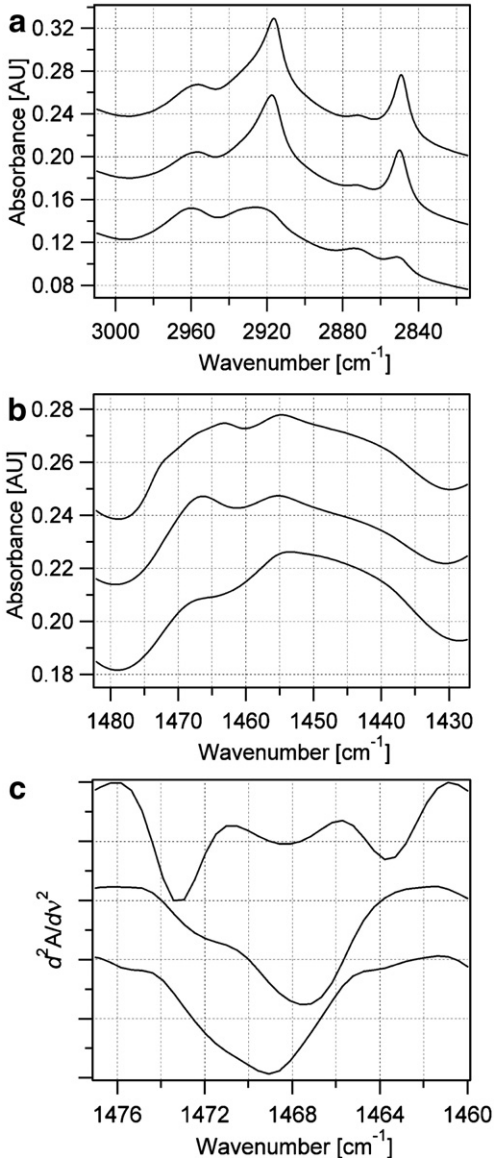

Fig. 5. Comparison of the spectroscopic features of human, porcine, and reconstructed skin. Representative examples of absorbance (a and b) and second-derivative (c) spectra collected at 32 °C from excised abdominal human skin (top spectra), excised porcine ear skin (middle spectra), and reconstructed human skin (bottom spectra). The spectra are offset for clarity.

3.3. Comparison of the lateral molecular organization of SC lipids in human, porcine, and reconstructed skin

Using the scissoring bandwidth FW-50, we compared the organization of the lipids in human SC with those in SC from porcine ear skin and from reconstructed skin—two substrates often used as models for human skin to study its interactions with topically applied substances [49–51]. Fig. 5 shows representative examples of absorbance (Fig. 5, a and b) and second-derivative (Fig. 5c) spectra of the three substrates collected at 32 °C, the typical temperature of the exposed surfaces of human skin *in vivo* [52].

In reconstructed SC both the overall content of lipids (estimated from the integrated intensities of the CH_2 stretching and scissoring modes) and the relative content of lipids and proteins (estimated from the relative intensities of the CH_2 and CH_3 stretching modes) were lower than those in human and porcine SC [53]. Apparently, the reconstructed SC has incorporated only a small amount of lipids in its structure, most probably due to the lack of lipidic ingredients in the growth medium used for this cell culture (information from the supplier).

The molecular organization in the three substrates at 32 °C differed considerably. In the spectra of human SC, the scissoring width of 11.7 ± 0.2 cm^{-1} and the position of the CH_2 symmetric stretching mode at 2849.39 ± 0.16 cm^{-1} indicated high content of lipids organized in an OR lattice, and a high overall degree of conformational order in the ensemble of lipid chains (average values± one standard deviation of nine samples from different donors). The corresponding values observed in porcine SC were 6.4 ± 0.8 cm^{-1} and 2849.98 ± 0.15 cm^{-1}, indicating approximately 50% lower content of OR phase and higher conformational disorder of the lipid chains than for lipids in human SC (average values±one standard deviation of nine samples from different donors). In spectra of reconstructed SC, these values were 5.9 ± 0.2 cm^{-1} and 2850.62 ± 0.51 cm^{-1}, respectively (average values±one standard deviation of six different cell cultures). While the scissoring widths measured in spectra of porcine and reconstructed SC were very close, the contours of the scissoring region in their second-derivative spectra differed considerably (Fig. 5c). In the spectrum of reconstructed SC, the shapeless, broad peak lacked the pronounced shoulder around 1472 cm^{-1} present in the spectrum of porcine SC, and was blue-shifted by ~1 cm^{-1}. Taken together with the position of the CH_2 symmetric stretching mode–one typical for considerably disordered lipid chains–this result indicated that the lipids in the reconstructed SC were organized predominantly in LIQ phases, possibly with some presence of HEX phases: this organization is drastically different from the one found in human SC.

We must underline that a comparison of the absolute values of the scissoring bandwidth in multicomponent samples of different composition has to be made with caution, since the magnitude of the scissoring split depends not only on the extent of the OR phase but also on the chain length and the number of hydrocarbon chains in the molecules forming this phase [27]. The overall composition of the lipid matrix in human and porcine SC, however, is sufficiently similar to tolerate our semi-quantitative comparison [1].

To gather further insight into the molecular organization of the three substrates, we compared the temperature dependence of the scissoring bandwidth FW-50 (Fig. 6, a and b) and of the position of the CH_2 symmetric stretching mode (Fig. 6c) in spectra collected while heating the samples from 28 to 90 °C. The temperature profile of the scissoring bandwidth in the three samples was very different. The bandwidth–and thus, the content of OR phase–in the human SC decreased by only 10% between 28 and 34 °C, followed by a steep decrease by more than 80% between 34 and 49 °C. Apparently, the composition and the organization of the lipid lamellae and the lipid envelope of the corneocytes in human SC have adapted to ensure a high content of ordered OR phases at temperatures close to the physiological temperature of exposed human skin; the transition from mostly

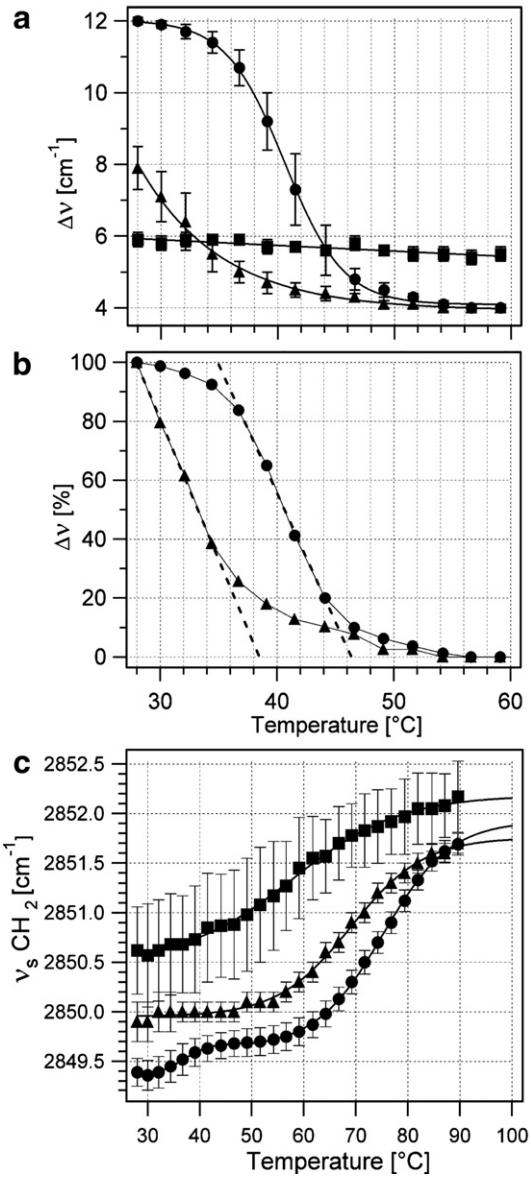

Fig. 6. Thermotropic phase transitions of the SC lipids in human, porcine, and reconstructed skin. Temperature dependence of the scissoring bandwidth FW-50 (a and b) and of the position of the CH_2 symmetric stretching vibration (c) in spectra collected from excised human abdominal skin (circles), excised porcine ear skin (triangles), and reconstructed skin (squares). The data points represent average±one standard deviation of the values estimated in spectra collected from different skin samples (samples from nine different donors for human and porcine skin, and six different reconstructed skin cell cultures). The data in panel (b) correspond to the data for human and porcine skin plotted in panel (a), normalized to their maximal bandwidth values (*i.e.*, the bandwidth measured at 28 °C; see text for details). The lines in panel (a) represent the best fits to the data points: a sigmoidal curve for the data from human skin (inflection point at 40.6± 0.1 °C), an exponential curve for the data from porcine skin, and a line for the data from reconstructed skin. The lines in panel (b) are for guidance of the eye only. The lines in panel (c) represent the best fits to the data points: two sigmoidal curves (28–50 °C and 50–100 °C, corresponding to the pre- and the main phase transitions, respectively) for the data from human skin, and one sigmoidal curve for the data from porcine and reconstructed skin.

OR to mostly HEX phases occurs at higher than physiological temperatures, in the range 34–49 °C. In the porcine SC, the scissoring bandwidth at *human* physiological temperatures was approximately 50% lower than the one observed in human SC; upon heating, it decreased gradually up to ~49 °C where it reached the same value as the human SC. We have found no data in the literature on the physiological temperature of the porcine ear; it, however, is most probably lower than the one of exposed human skin, as the vascularization of the ear is very sparse. Thus, it is possible that the distribution of the lipid classes between the lipid lamellae and the corneocyte envelopes (and possibly small variations of the composition of the SC lipids) in the porcine ear SC are tuned to ensure appropriately high content of crystalline OR phases at *its* physiological temperatures, *i.e.*, below 28 °C. Interestingly, the rate of decrease of the normalized scissoring bandwidth in porcine SC in the range 28–34 °C was very close to the rate of decrease of the corresponding bandwidth in human SC at higher temperatures, *i.e.*, in the range 37–44 °C (Fig. 6b). This similarity most probably reflects melting of lipid phases of similar composition, present in the two samples to a different extent [39].

Not surprisingly, the bandwidth in the reconstructed SC remained unchanged over the whole temperature interval. As shown in Fig. 5, due to their abnormal composition, the lipids in the reconstructed SC were initially organized predominantly in LIQ phases, possibly with a small content of HEX phase. As lateral chain organization was already absent at 28 °C, heating of the sample led only to further increase of the content of *gauche* conformers in the lipid chains.

The thermotropic changes of the position of the CH_2 symmetric stretching mode–reflecting the conformational order of the lipids chains–further confirmed our observations (Fig. 6c). In human SC, we observed the OR–HEX transition in the temperature range 28–50 °C (midpoint at 37.0±0.4 °C); concomitantly with the decrease of the scissoring bandwidth, it resulted in a small increase of the CH_2 symmetric stretching frequency (2849.36±0.15 to 2849.70±0.14 cm^{-1}). This pre-transition temperature was very close to the one calculated using a sigmoidal fit of FW-50 (40.6± 0.1 °C) and fully agrees with the published literature values [1]. Upon further increase of the temperature, we observed in addition the HEX–LIQ (*i.e.*, main) transition (midpoint at 75.2±0.2 °C), which resulted in a large increase of the CH_2 symmetric stretching frequency (2849.70±0.14 to 2851.69±0.11 cm^{-1}). In porcine SC, we observed clearly only the HEX–LIQ phase transition, with a midpoint of 69.0±0.4 °C. As expected from Fig. 6a, in this substrate the OR phases were initially present to a lesser extent compared to HEX phases; thus, the transition OR–HEX was practically masked by the relatively high CH_2 symmetric stretching frequency of the lipids organized in HEX phases. In reconstructed SC, the increase of the temperature led to a gradual increase of the CH_2 symmetric stretching frequency (2850.62± 0.44 to 2852.17±0.3 cm^{-1}), reflecting further disordering of the lipid chains within the LIQ phase.

In summary, using the scissoring bandwidth as a yardstick, we have demonstrated that the lateral molecular organization of the lipids in the topmost SC from human, porcine, and reconstructed skin differ significantly: the lipids form predominantly OR phases (mixed with some HEX ones) in human SC from abdominal skin, predominantly HEX phases (mixed with some OR ones) in porcine SC from ear skin, and predominantly LIQ phases (mixed with some HEX ones) in reconstructed SC from

one commercial supplier. Overall, our results are in agreement with the published data on the lateral molecular organization of mammalian and reconstructed skin. We must underline, however, that our conclusions concern only the topmost layer of the SC with a thickness determined by the penetration depth of the evanescent field probing the sample (in our experimental setup, this depth varied from 0.7 μm at 2850 cm^{-1} to 1.4 μm at 1460 cm^{-1}, assuming a refractive index of 1.5 for the skin and an angle of incidence of the IR beam equal to 45°). Several studies have suggested that the molecular organization is not homogeneous throughout the SC thickness and at different anatomical sites [48,54]. Currently, we are using the strategy presented here to establish the depth profile of the molecular organization of SC lipids in human skin *in vivo*.

3.4. Influence of propylene glycol and oleic acid on the SC lipid organization in excised human skin

Using second-derivative ATR-FTIR spectroscopy, we compared the effect of propylene glycol (PG) and oleic acid (OA) on excised human skin, a substrate of particular interest for the areas of dermatology, cosmetics, and transdermal drug delivery. These chemicals have been shown to interact with SC by different mechanisms: PG, often used as a co-solvent in topical formulations, interacts mostly with the SC keratins and does not alter significantly the SC lipid organization [55,56], while OA, a widely used penetration enhancer, is thought to create a highly permeable, fluid-like phase that co-exists with the endogenous SC lipids [57,58].

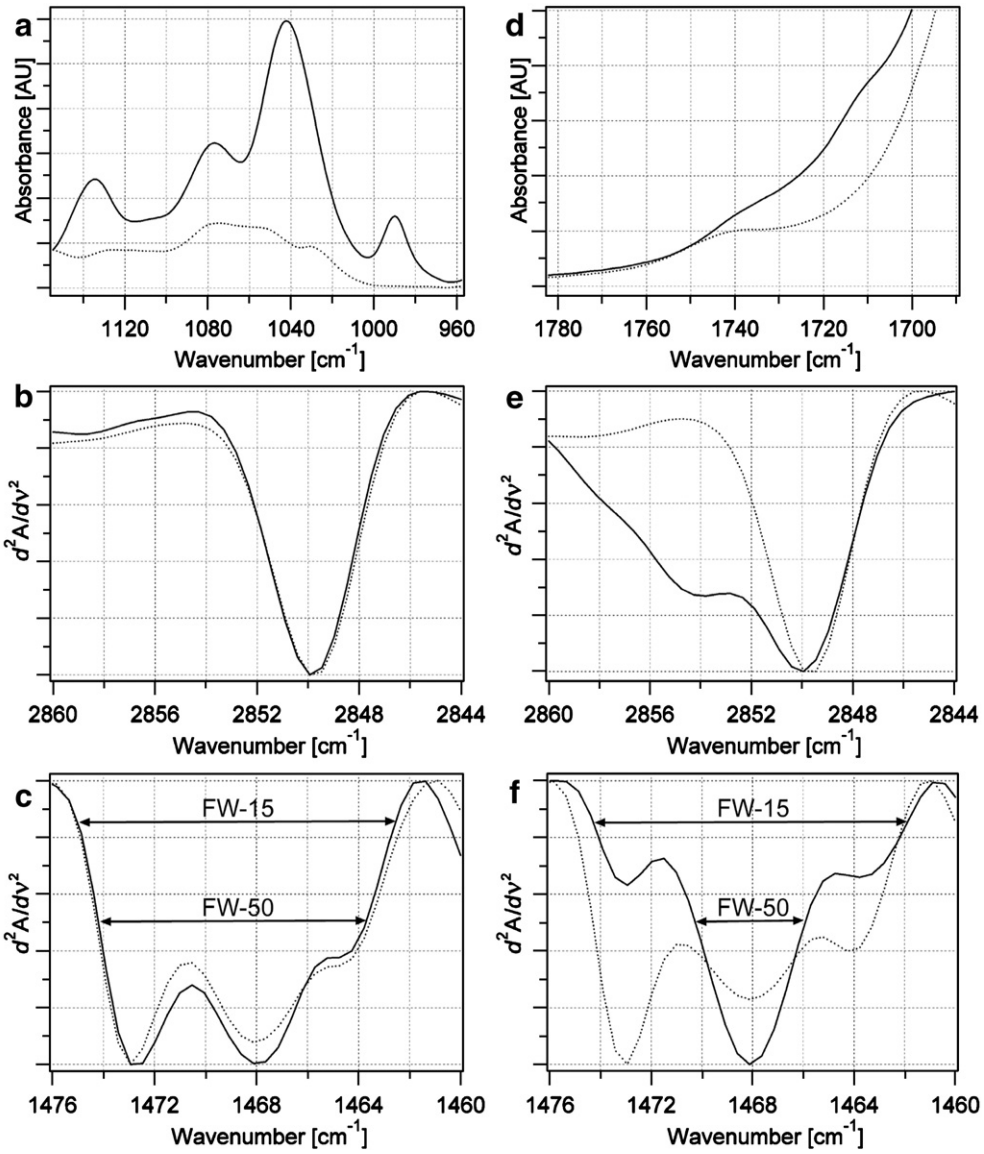

Fig. 7. Influence of PG and OA on the molecular organization of the lipids in human SC. Absorbance and second-derivative spectra collected at 32 °C from excised human skin after treatment with PG (a–c) and OA (d–f). The spectra shown with dotted lines in each panel were collected from the same skin sample in a control experiment (for details, see Materials and methods). The arrows in panels (c) and (f) denote the scissoring bandwidths measured at 50 and 15% of the peak height (FW-50 and FW-15, respectively). The second-derivative spectra were normalized to identical minima and maxima; those in panels (c) and (f) were in addition baseline-corrected.

Fig. 7 shows representative examples of absorbance and second-derivative spectra collected after treatment of excised human skin with PG and with ethanolic OA solution for 4 h, together with spectra of untreated skin collected after its incubation under the same conditions as the samples treated with PG and OA (for details, see Materials and methods). Both PG and OA incorporated into the SC, as seen from the relative increase of the absorbance around 1040 cm^{-1} (corresponding to the C–O stretching vibration of PG, Fig. 7a) and 1710 cm^{-1} (corresponding to the C=O stretching vibration of OA, Fig. 7d), respectively. Predictably, the incubation of skin with the two chemicals had very different effects on the conformational order of the SC lipid chains (Fig. 7, b and e). The position and the width of the CH_2 symmetric stretching band remained unchanged after incubation with PG; this observation implied the preservation of the conformational order of the SC lipids. Incubation with OA led to a slight blue shift of the main peak position, and the appearance of a massive shoulder at approximately 2854 cm^{-1}; this observation implied minor conformational disordering of a fraction of the SC lipid chains and the formation of a new, highly disordered phase.

Fig. 7, c and f shows the CH_2 scissoring region of representative second-derivative spectra collected from the skin surface after incubation with PG (Fig. 7c) and OA (Fig. 7f). The overall contour of the scissoring mode was similar to the one observed in the control samples: it contained the two components characteristic of OR phases–centered around 1473 and 1464 cm^{-1}–together with the component characteristic of HEX or LIQ phases—centered around 1468 cm^{-1}. The relative intensity of the three peaks, however, differed considerably: treatment with PG led to only a slight increase of the intensity at 1468 cm^{-1} compared to the intensities at 1473 and 1464 cm^{-1}, while after treatment with OA this increase was substantial. This result is fully consistent with the hypothesis that OA forms a separate, fluid-like phase within the SC lipids [57]. As a consequence, the scissoring bandwidth measured at 50% of the peak height (FW-50) comprised all three peaks after incubation with PG, but only the peak centered around 1468 cm^{-1} after incubation with OA. In contrast, the scissoring bandwidth measured at 15% of the peak height (FW-15) included contributions from all three peaks after incubation with both PG and OA.

To evaluate the degree of perturbation of the lateral lipid organization induced by the two chemicals, we compared their influence on the scissoring bandwidth with the effect of temperature on this parameter. Fig. 8 shows the scissoring bandwidth (FW-50 in Fig. 8a and FW-15 in Fig. 8b) of second-derivative spectra collected during the heating experiments described in Fig. 6, together with the corresponding values of FW calculated for the control samples. Because these samples were more hydrated than the samples used in the heating experiments, their FW values corresponded to those of untreated (drier) skin samples heated to approximately 37 °C; this result is consistent with previous observations [26]. Regardless of the peak height used to evaluate the scissoring bandwidth, the effect of incubation of excised human skin with PG was negligible within the experimental uncertainty. As expected from the data in Fig. 7, the two sides of the effect of OA on skin were exemplified at

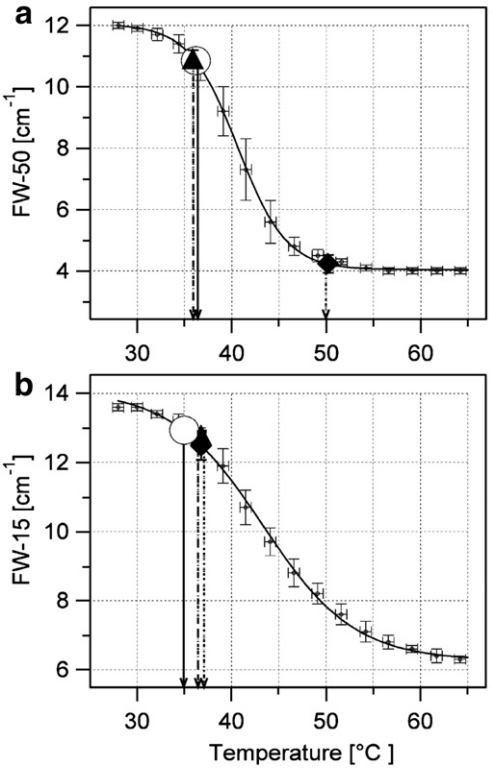

Fig. 8. Comparison of the effect of temperature, PG, and OA on the molecular organization of lipids in the SC of human skin. Values of FW-50 (a) and FW-15 (b) for untreated skin heated from 28 °C to 60 °C (dots; data from Fig. 6 a), skin treated with PG (triangles) and OA (diamonds) for 4 h, and control samples incubated for 4 h under the same conditions as the treated samples, without application of product (empty circles). All values represent average±one standard deviation obtained using skin samples from different donors (number of samples $n=9$ for untreated skin, $n=4$ for control samples, $n=3$ for samples treated with PG or OA). The lines indicate the temperatures corresponding to the values of FW for samples measured at 32 °C: full line for control samples, dashed line for skin treated with PG, and dotted line for skin treated with OA.

different peak heights. The formation of a disordered, OA-rich phase–corresponding to heating of the skin lipids to ≥50 °C–was best seen using FW-50 (Fig. 8a): this peak height included only the scissoring peak centered at 1468 cm^{-1} which arises mostly from OA incorporated in the SC. The lateral organization of another fraction of SC lipids–undistinguishable from the control sample within the experimental uncertainty–was demonstrated using FW-15 (Fig. 8b): this peak height included contributions from the peak arising mostly from OA (centered around 1468 cm^{-1}) and from the peaks from SC lipids organized in OR phases (centered around 1473 and 1464 cm^{-1}).

Our results demonstrate that the temperature dependence of the scissoring bandwidth is a useful yardstick against which to compare the effect of topically applied substances on the lateral organization of SC lipids. Furthermore, the appropriate selection of the height used for determination of the bandwidth allows one to distinguish between chemicals that disorder the OR lipid phases of the SC and those that form separate disordered phases. Even though quantitatively this discrimination is best achieved using radiolabeled or deuterated compounds [56], the approach we propose can give a useful first idea of the interactions between chemicals and SC lipids.

4. Discussion

This work describes a method for semi-quantitative evaluation of the lateral lipid chain packing in intact *Stratum corneum*, based on second-derivative spectroscopy. We have demonstrated that the scissoring bandwidth provides an easily accessible and reliable spectroscopic measure for the presence and the extent of OR and HEX phases.

In previous studies of the molecular organization in SC, ATR-FTIR spectroscopy has been used mostly to establish the conformational order of the lipid chains and the secondary structure of the SC keratins [8,59]. The use of this technique to also study the lateral organization in the SC lipid lamellae has two major advantages. First, it can be applied to full-thickness skin, both *in vivo* and *ex vivo*; no separation of the *Stratum corneum* from the underlying skin layers, or drying of the sample is required before recording an ATR-FTIR spectrum. Second, the penetration depth of the incident IR beam limits the thickness of the surface layer that is sampled; thus, contrary to transmission FTIR studies, the information regarding the lateral organization of the SC lipids is not averaged over the full SC thickness. Combined with tape-stripping or using ATR crystals with different refractive indices (thus enabling probing of the skin at different depths [37,42,60]), our approach is suitable for depth profiling of the SC lipid organization.

The procedure we described also permits evaluation of the changes induced in the lateral organization of the SC lipids by topical application of products and provides information about the molecular basis of the interactions. The exact correlation between the overall structure of the SC, the molecular organization of the SC lipid matrix, and the normal barrier properties of human skin is as yet unclear. Several studies have demonstrated that the conformational order of the SC lipids modulates the skin permeability for water [17] and small molecules [42]; the role of the lateral lipid organization for permeability is not well understood [61]. We believe that the combination of *in vivo* ATR-FTIR studies of the molecular conformation and lateral organization with functional measurements of the barrier function (*e.g.,* trans-epidermal water loss, TEWL [17], or skin electrical impedance [62]) is a promising approach to study the molecular requirements for an efficient skin barrier to water evaporation and to penetration of exogenous substances.

Acknowledgement

We thank Christian Margot for many helpful discussions and for critically reading the manuscript.

Appendix A. Supplementary data

Supplementary data associated with this article can be found, in the online version, at doi:10.1016/j.bbamem.2008.01.022.

References

[1] J.A. Bouwstra, M. Ponec, The skin barrier in healthy and diseased state, Biochim. Biophys. Acta—Biomembranes 1758 (2006) 2080–2095.
[2] C.R. Harding, The Stratum corneum: structure and function in health and disease, Dermatologic Therapy 17 (2004) 6–15.
[3] K.C. Madison, Barrier function of the skin: "La raison d'être" of the epidermis, J. Invest. Dermatol. 121 (2003) 231–241.
[4] G.S.K. Pilgram, A.M. Engelsma-van Pelt, J.A. Bouwstra, H.K. Koerten, Electron diffraction provides new information on human Stratum corneum lipid organization studied in relation to depth and temperature, J. Invest. Dermatol. 113 (1999) 403–409.
[5] K. Knutson, R.O. Potts, D.B. Guzek, G.M. Golden, J.E. McKie, W.J. Lambert, W.I. Higuchi, Macro- and molecular physicochemical considerations in understanding drug transport in the Stratum corneum, J. Contr. Release 2 (1985) 67–87.
[6] L. Brancaleon, M.P. Bamberg, N. Kollias, Spectral differences between Stratum corneum and sebaceous molecular components in the mid-IR, Appl. Spectr. 54 (2000) 1175–1182.
[7] G.W. Lucassen, G.N.A. van Veen, J.A.J. Jansen, Band analysis of hydrated human skin Stratum corneum attenuated total reflectance Fourier transform infrared spectra in vivo, J. Biomed. Optics 3 (1998) 267–280.
[8] K. Babita, V. Kumar, V. Rana, S. Jain, A.K. Tiwary, Thermotropic and spectroscopic behavior of skin: Relationship with percutaneous permeation enhancement, Curr. Drug Deliv. 3 (2006) 95–113.
[9] N. Kitson, J. Thewalt, M. Lafleur, M. Bloom, A model membrane approach to the epidermal permeability barrier, Biochemistry 33 (1994) 6707–6715.
[10] D.C. Swartzendruber, P.W. Wertz, D.J. Kitko, K.C. Madison, D.T. Downing, Molecular models of the intercellular lipid lamellae in mammalian Stratum corneum, J. Invest. Dermatol. 92 (1989) 251–257.
[11] B. Forslind, A domain mosaic model of the skin barrier, Acta Derm. Venereol. 74 (1994) 1–6.
[12] B. Forslind, S. Engstroem, J. Engblom, L. Norlen, A novel approach to the understanding of human skin barrier function, J. Dermatol. Sci. 14 (1997) 115–125.
[13] M. Lafleur, Phase behaviour of model Stratum corneum lipid mixtures: an infrared spectroscopy investigation, Can. J. Chem. 76 (1998) 1501–1511.
[14] M. Arseneault, M. Lafleur, Cholesterol-sulfate and Ca^{2+} modulate the mixing properties of lipids in Stratum corneum model mixtures, Biophys. J. 92 (2007) 99–114.
[15] D.J. Moore, M.E. Rerek, Insight into the molecular organization of lipids in the skin barrier from infrared spectroscopy studies of Stratum corneum lipid models, Acta Derm. Venereol. Supp. 208 (2000) 16–22.
[16] D.J. Moore, M.E. Rerek, R. Mendelsohn, FTIR spectroscopy studies of the conformational order and phase behavior of ceramides, J. Phys. Chem. B 101 (1997) 8933–8940.
[17] R.O. Potts, M.L. Francoeur, Lipid biophysics of water loss through the skin, Proc. Natl. Acad. Sci. U. S. A. 87 (1990) 3871–3873.
[18] A.V. Rawlings, P.J. Matts, Stratum corneum moisturization at the molecular level: An update in relation to the dry skin cycle, J. Invest. Dermatol. 124 (2005) 1099–1110.
[19] S.L. Krill, K. Knutson, W.I. Higuchi, The Stratum corneum lipid thermotropic phase behavior, Biochim. Biophys. Acta 1112 (1992) 281–286.
[20] S.T.K. Narishetty, R. Panchagnula, Effect of L-menthol and 1,8-cineole on phase behavior and molecular organization of SC lipids and skin permeation of Zidovudine, J. Contr. Release 102 (2005) 59–70.
[21] R.N.A.H. Lewis, R.N. McElhaney, FTIR spectroscopy in the study of hydrated lipids and lipid bilayer membranes, in: H.H. Mantsch, D. Chapman (Eds.), Infrared Spectroscopy of Biomolecules, Wiley-Liss, Inc., 1996.
[22] R.A. Dluhy, B.Z. Chowdhry, D.G. Cameron, IR characterization of conformational differences in the lamellar phases of DPPC, Biochim. Biophys. Acta 821 (1985) 437–444.
[23] J. Umemura, D.G. Cameron, H.H. Mantsch, A FTIR study of the molecular interaction of cholesterol with DPPC, Biochim. Biophys. Acta 602 (1980) 32–44.
[24] J.A. Bouwstra, A. de Graaff, G.S. Gooris, J. Nijsse, J.W. Wiechers, A.C. van Aelst, Water distribution and related morphology in human Stratum corneum at different hydration levels, J. Invest. Dermatol. 120 (2003) 750–758.
[25] B. Ongpipattanakul, M.L. Francoeur, R.O. Potts, Polymorphism in Stratum corneum lipids, Biochim. Biophys. Acta 1190 (1994) 115–122.

[26] C.L. Gay, R.H. Guy, G.M. Golden, V.H.W. Mak, M.L. Francoeur, Characterization of low-temperature (i.e., <65 °C) lipid transitions in human Stratum corneum, J. Invest. Dermatol. 103 (1994) 233–239.
[27] D.G. Cameron, E.F. Gudgin, H.H. Mantsch, Dependence of acyl chain packing of phospholipids on the head group and acyl chain length, Biochemistry 20 (1981) 4496–4500.
[28] D.J. Moore, R.G. Snyder, M.E. Rerek, R. Mendelsohn, Kinetics of membrane raft formation: fatty acid domains in Stratum corneum lipid models, J. Phys. Chem. B 110 (2006) 2378–2386.
[29] R.D. Pensack, B.B. Michniak, D.J. Moore, R. Mendelsohn, Infrared kinetic/structural studies of barrier reformation in intact Stratum corneum following thermal perturbation, Appl. Spectr. 60 (2006) 1399–1404.
[30] C. Ricci, K.L.A. Chan, S.G. Kazarian, Combining the tape-lift method and FTIR imaging for forensic applications, Appl. Spectr. 60 (2006) 1013–1021.
[31] G.W. Lucassen, P.J. Caspers, G.J. Puppels, Water content and water profiles in skin measured by FTIR and Raman spectroscopy, Proc. SPIE 4162 (2000) 39–45.
[32] L. Brancaleon, M.P. Bamberg, T. Sakamaki, N. Kollias, ATR-FTIR spectroscopy as a possible method to investigate biophysical parameters of Stratum corneum in vivo, J. Invest. Dermatol. 116 (2001) 380–386.
[33] R.O. Potts, D.B. Guzek, R.R. Harris, J.E. McKie, A non-invasive, in vivo technique to quantitatively measure water concentration of the Stratum corneum using ATR IR spectroscopy, Arch. Dermatol. Res. 277 (1985) 489–495.
[34] J.E. Harrison, A.C. Watkinson, D.M. Green, J. Hadgraft, K. Brain, The relative effect of Azone and Transcutol on permeant diffusivity and solubility in human Stratum corneum, Pharm. Res. 13 (1996) 542–546.
[35] A.L. Stinchcomb, F. Pirot, G.D. Touraille, A.L. Bunge, R.H. Guy, Chemical uptake into human Stratum corneum in vivo from volatile and non-volatile solvents, Pharm. Res. 16 (1999) 1288–1293.
[36] H.M. Heise, L. Kuepper, W. Pittermann, L.N. Butvina, New tool for epidermal and cosmetic formulation studies by ATR spectroscopy using a flexible mid-infrared fiber probe, Fresenius J. Anal. Chem. 371 (2001) 753–757.
[37] K.L.A. Chan, S.G. Kazarian, ATR FTIR imaging with variable angle of incidence: A three-dimensional profiling of heterogeneous materials, Appl. Spectr. 61 (2007) 48–54.
[38] K.L.A. Chan, S.G. Kazarian, Chemical imaging of Stratum corneum under controlled humidity with ATR-FTIR spectroscopy method, J. Biomed. Optics 12 (2007) 044010.
[39] G. Ungar, N. Masic, Order in the rotator phase of *n*-alkanes, J. Phys. Chem. 89 (1985) 1036–1042.
[40] H.H. Mantsch, D.J. Moffatt, H.L. Casal, Fourier transform methods for spectral resolution enhancement, J. Molec. Str. 173 (1988) 285–298.
[41] D.M. Small, Lateral chain packing in lipids and membranes, J. Lipid Res. 25 (1984) 1490–1500.
[42] V.H.W. Mak, R.O. Potts, R.H. Guy, Percutaneous penetration enhancement in vivo measured by ATR-IR spectroscopy, Pharm. Res. 7 (1990) 835–841.
[43] H. Tanojo, E. Boelsma, H.E. Junginger, M. Ponec, H.E. Bodde, In vivo human skin barrier modulation by topical application of fatty acids, Skin Pharmacol. Appl. Skin Physiol. 11 (1998) 87–97.
[44] D.G. Cameron, J.K. Kauppinen, D.J. Moffatt, H.H. Mantsch, Precision in condensed phase vibrational spectroscopy, Appl. Spectr. 36 (1982) 245–250.
[45] H. Margeneau, G. Murphy, The Mathematics of Physics and Chemistry, 2D. van Nostrand Co., Princeton, N.J., 1964
[46] H. Nouar, D. Petitjean, M. Bouroukba, M. Dirand, Binary phase diagram of the system *n*-docosane–*n*-tricosane, J. Molec. Str. 443 (1998) 197–204.
[47] R.G. Snyder, M.C. Goh, V.J.P. Srivatsavoy, H.L. Strauss, D.L. Dorset, Measurement of the growth kinetics of microdomains in binary *n*-alkane solid solutions by infrared spectroscopy, J. Phys. Chem. 96 (1992) 10008–10019.
[48] D. Bommannan, R.O. Potts, R.H. Guy, Examination of the effect of ethanol on Stratum corneum in vivo using infrared spectroscopy, J. Contr. Release 16 (1991) 299–304.
[49] C. Herkenne, A. Naik, Y.N. Kalia, J. Hadgraft, R.H. Guy, Pig ear skin ex vivo as a model for in vivo dermatopharmacokinetic studies in man, Pharm. Res. 23 (2006) 1850–1856.
[50] R. Pouliot, L. Germain, F.A. Auger, N. Tremblay, J. Juhasz, Physical characterization of the Stratum corneum of an in vitro human skin equivalent produced by tissue engineering and its comparison with normal human skin by ATR-FTIR spectroscopy and thermal analysis (DSC), Biochim. Biophys. Acta 1439 (1999) 341–352.
[51] H.M. Reinl, A. Hartinger, P. Dettmar, T.M. Bayerl, Time-resolved infrared ATR measurements of liposome transport kinetics in human keratinocyte cultures and skin reveals a dependence on liposome size and phase state, J. Invest. Dermatol. 105 (1995) 291–295.
[52] E.F.J. Ring, Thermal imaging of skin temperature, in: J. Serup, G.B.E. Jemec (Eds.), Handbook of Non-invasive Methods and the Skin, CRC Press, Inc., Boca Raton, FL, 1995.
[53] R. Mendelsohn, H.-C. Chen, M.E. Rerek, D.J. Moore, Infrared micro-spectroscopic imaging maps the spatial distribution of exogenous molecules in skin, J. Biomed. Optics 8 (2003) 185–190.
[54] H.E. Bodde, L.A.R.M. Pechtold, F.H.N. de Haan, A large-scale non-invasive in vivo screening of the human barrier recording ATR-FTIR spectra, TEWL, skin impedance and temperature, Proc. Internat. Symp. Control. Rel. Bioact. Mater. 18 (1991) 311–312.
[55] S.-Y. Lin, K.-J. Duan, T.-C. Lin, Microscopic FTIR/DSC system used to simultaneously investigate the conversion process of protein structure in porcine Stratum corneum after pretreatment with skin penetration enhancers, Meth. Find. Exp. Clin. Pharmacol. 18 (1996) 175–181.
[56] V.H.W. Mak, R.O. Potts, R.H. Guy, Oleic acid concentration and effect in human Stratum corneum: non-invasive determination by ATR-IR in vivo, J. Contr. Release 12 (1990) 67–75.
[57] B. Ongpipattanakul, R.R. Burnette, R.O. Potts, M.L. Francoeur, Evidence that oleic acid exists in a separate phase within Stratum corneum lipids, Pharm. Res. 8 (1991) 350–354.
[58] A.C. Rowat, N. Kitson, J.L. Thewalt, Interactions of oleic acid and model Stratum corneum membranes as seen by ^{2}H NMR, Int. J. Pharmaceut. 307 (2006) 225–231.
[59] A. Naik, R.H. Guy, Infrared spectroscopic and differential scanning calorimetric investigations of the Stratum corneum barrier function, in: R.O. Potts, R.H. Guy (Eds.), Mechanisms of transdermal drug delivery, Marcel Dekker, NY, 1997.
[60] C. Laugel, C. Do Nascimento, D. Ferrier, J.P. Marty, A. Baillet, Contribution of ATR-FTIR spectroscopy for studying the in vitro behavior of octylmethoxycinnamate after topical application, Appl. Spectr. 55 (2001) 1173–1180.
[61] I.W.H.M. Craane-Van Hisberg, J. Coos Verhoef, F. Spies, J.A. Bouwstra, G.S. Gooris, H.E. Junginger, H.E. Bodde, Electroperturbation of the human skin barrier in vitro: II. Effects of Stratum corneum lipid ordering and ultrastructure, Microsc. Res. Techn. 37 (1998) 200–213.
[62] P. Karande, A. Jain, S. Mitragotri, Relationship between skin's electrical impedance and permeability in the presence of chemical enhancers, J. Contr. Release 110 (2006) 307–313.